Significance tests on the output power of a thermally driven rotary nanomotor

2017 Nanotechnology 28 215705

(http://iopscience.iop.org/0957-4484/28/21/215705)

IOP Publishing

Nanotechnology

Nanotechnology **28** (2017) 215705 (8pp)

https://doi.org/10.1088/1361-6528/aa6961

Significance tests on the output power of a thermally driven rotary nanomotor

Likui Yang[1], **Kun Cai**[1,2,3], **Jiao Shi**[1] **and Qing H Qin**[2,3]

[1] College of Water Resources and Architectural Engineering, Northwest A&F University, Yangling 712100, People's Republic of China

[2] Research School of Engineering, the Australian National University, ACT, 2601, Australia

E-mail: kuncai99@163.com and qinghua.qin@anu.edu.au

Received 2 March 2017, revised 19 March 2017
Accepted for publication 27 March 2017
Published 4 May 2017

CrossMark

Abstract

Many factors can have a significant influence on the output power of a thermally driven rotary nanomotor made of carbon nanotubes (CNTs). Making use of a computational molecular dynamics approach, we evaluate for the first time the output power of a nanomotor, considering some of the main factors including temperature, the diameter of the rotor and the number of IRD atoms (*N*) on the stator. When applying extra-resistant torque to the rotor to let the stable value of the rotational frequency of the rotor fluctuate near zero, the value of the resistant torque can be considered as the output power of the rotor. The effects of these factors on the output power of a motor are roughly predicted via a fitting approach. Using stepwise regression analysis, we discover that *N* has the greatest influence on the output power. The second and the third main factors that affect the output power of a nanomotor are the diameter of the rotor, and the interaction between *N* and the diameter, respectively. To improve the output power of a nanomotor, one can place more IRD atoms in the system and/or employ CNTs with larger diameters.

Supplementary material for this article is available online

Keywords: nanomotor, nanotube, significance test, regression model, output power

(Some figures may appear in colour only in the online journal)

1. Introduction

In recent years, the fabrication of nanodevices [1–5] from low-dimensional materials [6–10] has attracted more and more attention from researchers. It should be mentioned that the Nobel prize for chemistry in 2016 was issued to three scientists for their contributions to molecular machines [11]. Carbon nanotubes (CNTs), since being discovered by transmission electron microscopy in the early 1990s [7], have been studied widely for their physical properties. Due to their excellent high modulus [12], high ductility [13] and ultra-low inter-tube friction [1, 14–16], CNTs are ideal candidate materials in fabricating various nanomachines such as nanomotors [1, 2, 17–21], nano strain sensors [22] and nano-oscillators [23–27]. In particular, Cumings and Zettl [1] developed a nanomotor by using multi-walled CNTs for the shaft of the rotor. Fennimore *et al* [2] used CNTs to support a plate which can be made to rotate by applying direct current. Bourlon *et al* [17] arranged a plate on the outer tube of multi-walled CNTs, whereby the plate can be driven to rotate by an external electric field. In the work by Barreiro *et al* [18], CNTs were employed as an axis through which the motion of a cargo can be driven by a thermal gradient along the tube axis. Besides experiments, a molecular dynamics simulation approach is also a powerful tool for investigating this category of nanodevices [19, 20, 27].

In 2014, the thermally-driven rotary nanomotor (TRnM) was created using double-walled CNTs [28]. In the nanomotor, the outer shell of the CNT is fixed as a stator after relaxation, and the inner tube is actuated to rotate at ~100 GHz. The mechanism involves the asymmetry of the stator leading to a torque moment on the rotor during their thermal vibration-induced collision. When the double-walled CNTs with a radii

[3] Authors to whom any correspondence should be addressed.

difference of 0.335 nm (the equilibrium distance between neighboring tubes) are chosen to act as a TRnM, the rotational frequency of the rotor is commonly lower than that of the nanomotor with the same stator, but the radii difference is near 0.335 nm. The reason for this is that the collision between the stator and the rotor is reduced when the radii difference is much lower or higher than that at equilibrium. It should be mentioned that the TRnM from the double-walled CNTs with unsaturated ends may stop rotating suddenly, even if it has a long stable rotation time [29]. From molecular dynamics experiments, the reason was found that the drastic vibration with high centrifugal force on the atoms attached to the rotor may lead to the formation of new carbon-carbon covalent bonds between the rotor and the stator. Under this extremely strong bonding interaction, the rotational speed of the rotor drops to zero within a few picoseconds. In early 2016, a model of the TRnM with a specified rotational direction was presented [30]. In the model, one or more unsaturated atoms at one end of the stator are initially set to have an inwardly radial deviation (IRD). When the collision between the rotor and stator happens, torque with a direction corresponding to the type of IRD is generated to actuate the rotation of the rotor. Due to the extremely small size of the nanomotor and ultra-high speed of the rotor, observation of the rotation is highly challenging. To deal with this difficulty, we suggested adding a piece of graphene nanoribbon to the rotor [31]. When the rotor is actuated, the nanoribbon will expand from the tube. The size of the rotor is enlarged and the rotational speed of the rotor reduced, simultaneously. This phenomenon is useful for experimental observation of the rotation. Based on this idea, we proposed a probe-based approach to measure the rotational frequency of a nanomotor [32, 33].

Having completed the measurement of the rotation, we now focus on the output power of the TRnM from CNTs when considering the function of the former in driving the motion of other components in a nanomachine. In the experiments above, the stable rotational frequency (SRF) of the rotor still shows high dependence on factors such as the geometry of the nanomotor and the temperature of the system. In the present study, we investigate the effects of factors including temperature, the diameter of the rotor and the number of IRD atoms on the output power of the TRnM, as shown in figure 1.

2. Models and methodology

2.1. Models of thermally driven nanomotor

See figure 1.

2.2. Outline of numerical experiments

The rotational frequency ω of the rotor in figure 1 is not equal to zero on time average when no resistant torque is applied to the left end of the rotor. The reason for this is that the collision between the rotor and the stators can provide uni-directional torque, which leads to the rotation of the rotor only on the condition that the stators have lost geometric symmetry, e.g., by setting IRD on some end carbon atoms on the stators (e.g., figure 1(b)). If we apply a torsional moment on the left end of the rotor and the directional sense of the moment is opposite to that of the rotation, the value of ω would change. For example, if the value of M_r is low, the value of ω will reduce, but the directional sense remains unchanged. If we provide a higher value of M_r on the rotor, it may rotate in the opposite way. Hence, we predict that there must exist a value of M_r which leads to $\omega = 0$ on time average. Correspondingly, the value of M_r is called a critical value and is labeled as M_r^{cr}.

In the present study, the major task is to find the significance of one factor or multiple factors on the output power (torque, reaction quantity of M_r^{cr}) of the thermally driven rotary nanomotor, as shown in figure 1. Hence, before conducting a factor analysis, the critical value of the resistant torque (M_r^{cr}) should be obtained under specific conditions. In a factor analysis, four major steps are required:

(a) Choose samples for analysis according to the factor to be estimated. For instance, when the factor is temperature, we need to obtain the critical values of torque of the same system at a different temperature.
(b) Build the related models involved in the factor analysis.
(c) Obtain the critical value of resistant torque for each case of simulation by a bi-section method.
(d) Collect the critical values of the resistant torque of the system with respect to different values of the factor(s), and carry out factor analysis using a software statistical analysis system (SAS) [35].

2.3. Method for molecular dynamics simulation

The simulation is carried out in an open source code large-scale atomic/molecular massively parallel simulator (LAMMPS) [36]. The interaction among the carbon and/or hydrogen atoms is described by the AIREBO potential [37]. In each simulation, the time step is 0.001 ps and there are five major steps required:

Step (1) Build the geometry model of the system, adjust the positions of the IRD atoms at the external ends of the stators.

Step (2) Reshape the nanosystem by minimizing the potential energy of the system using the steepest decent algorithm with a tolerance of 10^{-4} and 10^{-6} units for energy and force, respectively. The maximal iterations are 100 and 1000, respectively.

Step (3) Initiate the velocities of the atoms on the system with a specified temperature, e.g., 300 K.

Step (4) Fix the carbon atoms on the stators, apply a specified value of M_r to the three rings at the left end of the rotor, and place some free atoms on the rotor in a canonical NVT ensemble with a specified temperature.

Step (5) Run 20 million iterations and record data for post-processing, simultaneously.

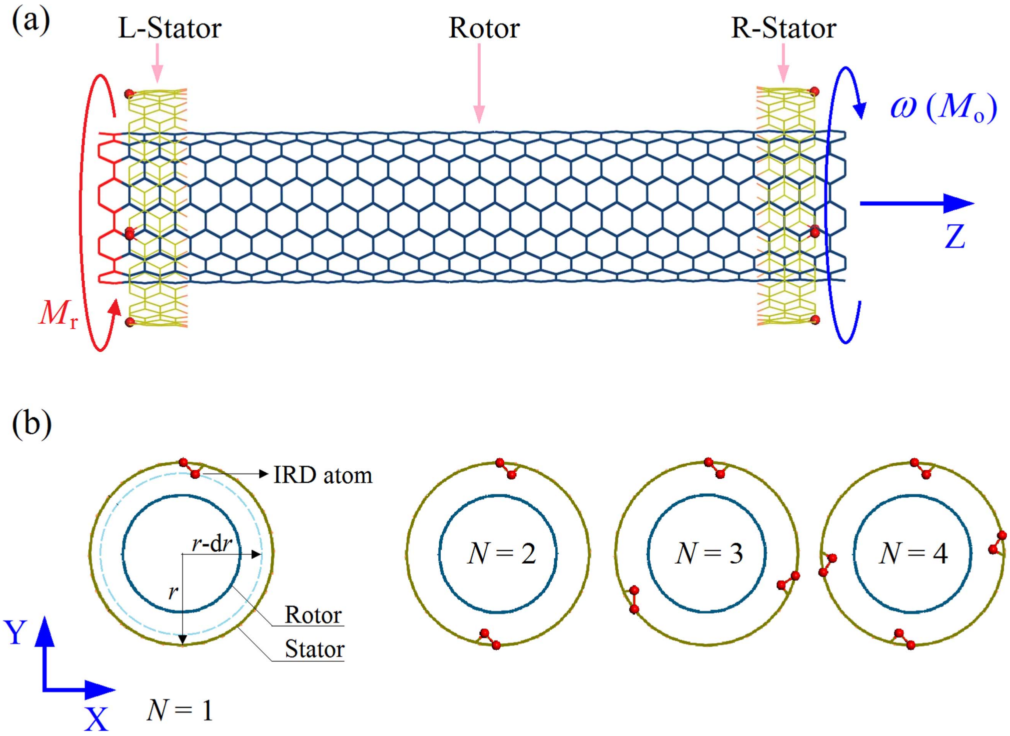

Figure 1. A schematic of a thermally driven rotary nanomotor made of armchair/armchair double-walled carbon nanotubes of $(n_i, n_i)/(n_o, n_o)$. To keep both tubes in an equilibrium state, the chirality parameters satisfy $n_o = n_i + 5$. The inner tube acts as a rotor and the outer tubes behave as stators (L-stator and R-stator). The internal ends of the stators are hydrogenated [34]. (a) A side-view of the system. The initial length of the rotor is ~6.15 nm, and the axial distance (along the *Z* direction) between the rotor and the external end of the stator is ~0.246 nm. ω is the output rotational frequency of the rotor when the magnitude of the resistant torque $M_r = 0$ is applied to the three rings at the left end of the rotor. The output torque $\boldsymbol{M}_o$ (i.e., the output power of the nanomotor) is equal but opposite to the resistant torque $\boldsymbol{M}_r$. (b) An axial view of the system along the negative *Z* direction. The red atoms at the external ends of the stators may have inward radial deviation (IRD) to actuate the rotation of the rotor; *N* is the number of IRD atoms on each stator. The IRD atoms have the same value of IRD, i.e., $\mathrm{d}r = 0.4 l_{c\text{-}c}$ with $l_{c\text{-}c} = 0.142$ nm [30].

2.4. Bi-section algorithm

The third step of the factor analysis aims to find out the critical value of the resistant torque for each case. The bi-section method is used in this analysis. The time-averaged rotational frequency of the rotor subjected to resistant torque M_r is labeled as ω (M_r). The method contains the following six steps:

(i) Determine the initial interval of M_r, e.g., (a, b) which satisfies $\omega(a) \times \omega(b) < 0$.
(ii) Let $c = (a + b)/2$, calculate $\omega(c)$.
(iii) If $|\omega(c)| < \min\{|\omega(0) \times 5\%|, 5\,\text{GHz}\}$, go to (vi); otherwise, go to (iv).
(iv) If $\omega(c) \times \omega\ (a) > 0$, let $a = c$; or $\omega(c) \times \omega(b) > 0$, let $b = c$.
(v) Judge: if $(b - a)/\max\{|a|, |b|\} < 0.1\%$, go to (vi); otherwise, go to (ii).
(vi) Stop and write down $M_r^{cr} = c$ and $\omega(M_r^{cr})$.

Generally, the critical value of M_r can be obtained after no more than ten iterations. The time-averaged value of ω is equal to the mean value of ω within the latest 2 ns, i.e., the time average is fulfilled in the time interval (18, 20) ns.

2.5. Description of factor analyses

To find the correlation between the major factors, e.g., the temperature, the chirality of the rotor and the number of IRD atoms, and the output torsional moment, we carry out both single factor and multi-factor analysis. As multi-factor analysis is based on single factor analysis, first, we begin by carrying out a single factor analysis on the temperature, the chirality of the rotor and the number of IRD atoms one by one; this is followed by the multi-factor analysis. The whole process is listed as follows:

Scheme (1) The temperature is considered to be the first factor to be evaluated. In this scheme, the nanomotor from (5, 5)/(10, 10), i.e., $n_i = 5$, is employed, and the number of IRD atoms $N = 1$. Both n_i and *N* are unchanged in exploring the temperature influence. Six samples are involved in the simulation: T = 100, 200, 300, 400, 500 and 600 K. The critical values of resistant torque M_r, rather than M_o, are recorded for late factor analysis.

Scheme (2) The next factor is the diameter or chirality parameter of the rotor (n_i, n_i). In this scheme, $N = 2$, $T = 300$ K, and eight nanomotors are involved. The values of n_i related to the nanomotors are listed in table 1, i.e., $n_i = 5$,

Table 1. The coding values of level of *T*, n_i and *N* in an orthogonal design. The 0-level is ignored.

Level	T	n_i	N
−1	$T_1 = 100$ K	$n_{i1} = 9$	$N_1 = 1$
1	$T_2 = 500$ K	$n_{i2} = 20$	$N_2 = 4$

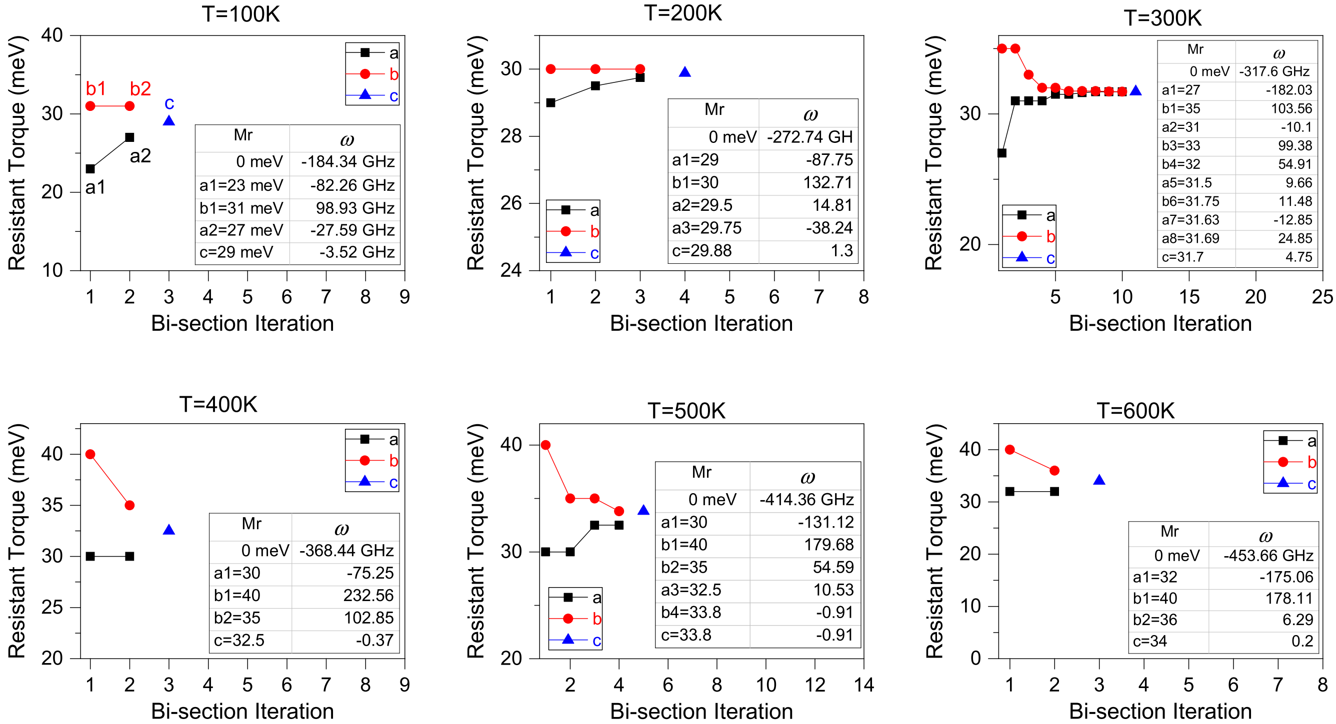

Figure 2. The iteration history of the critical value of the resistant torque (M_r^{cr}) on the rotor at different temperatures. Correspondingly, the SRF of rotor (ω) is given at each step of the bi-section algorithm.

7, 9, 12, 14, 16, 18 and 20. The critical values of resistant torque M_r are again recorded for late factor analysis.

Scheme (3) The third factor is N—the number of IRD atoms attached to the stator—and the influence of N is estimated. The nanomotor from (9, 9)/(14, 14) at 300 K is used, i.e., $n_i = 9$ and $T = 300$ K. N is assumed to be 1, 2, 3 and 4, respectively. The critical values of resistant torque M_r for the factor N are recorded for late factor analysis.

Scheme (4) Multi-factor regression orthogonal analysis is done in this scheme by considering three major factors simultaneously. To reduce the computational time and to maintain the reliability of estimation on the three factors, only eight samples are calculated with consideration of the three factors and the interaction between any two of them. The eight samples are processed by the SAS software for orthogonal experiments according to the results of a three-factor/two-level orthogonal design with $T = 100$ K and 500 K; $n_i = 9$ and 20; and $N = 1$ and 4. The details are described in section 3 below.

Having obtained the critical torque M_r^{cr}, of the samples, a significance analysis is carried out. In the present study, a hypothesis testing approach is used in the analysis on the effects of these factors on the output power of the rotor, which is equal but opposite to M_r^{cr}. For the convenience of the description, we consider M_r^{cr} as M_o directly. Generally, the significance of the factor(s) is indirectly expressed by the probability P, i.e., if $P < 0.05$, the samples are well selected with no more than 5% probability of the difference of the sample results being caused by the sample design. The factor effect can be validly estimated. In single factor analysis, linear regression is adopted to find the relationship between M_r^{cr}

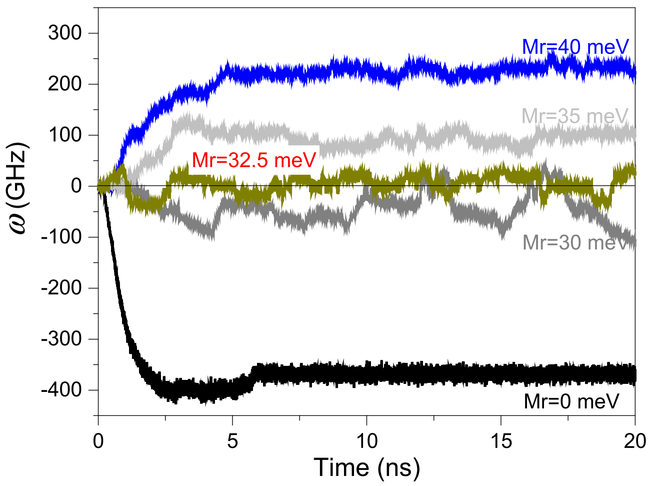

Figure 3. The history curves of the rotational frequency of the rotor (ω) under different resistant torque (M_r) at 400 K. The value of M_r^c equals 32.5 meV.

and each factor, and the multivariable nonlinear regression model is used in multi-factor analysis.

In a factor analysis at many levels, suppose the number of levels is k, and the number of observations at each level is r, X_{ij} is the jth observation at the ith level. The significant difference of factor A with respect to the observations (i.e., critical resistant torque) can be estimated according to the following equation:

$$F = \frac{S_A^2}{S_e^2} = \left(\frac{SS_A}{k-1}\right) \bigg/ \left(\frac{SS_e}{k(r-1)}\right), \tag{1}$$

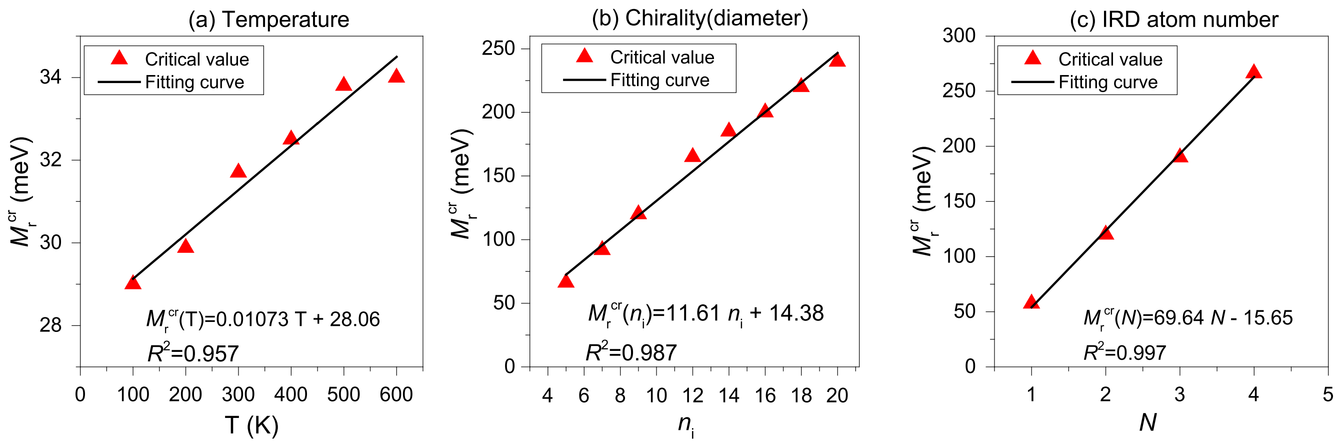

Figure 4. The linear fitting results of $M_r{}^{cr}$ with respect to different levels of the three factors, i.e., T, n_i and N.

Table 2. Coding table for orthogonal regression experiment.

Sample No.	$x_1 \sim T$	$x_2 \sim n_i$	$x_1 \times x_2$	$x_3 \sim N$	$x_1 \times x_3$	$x_1 \times x_3$	Vacancy
1	1	1	1	1	1	1	1
2	1	1	1	−1	−1	−1	−1
3	1	−1	−1	1	1	−1	−1
4	1	−1	−1	−1	−1	1	1
5	−1	1	−1	1	−1	1	−1
6	−1	1	−1	−1	1	−1	1
7	−1	−1	1	1	−1	−1	1
8	−1	−1	1	−1	1	1	−1

where SS_A and SS_e are the sums of the mean square of the model (with respect to factor A) and the error, respectively, and can be calculated using the following equations:

$$SS_A = \frac{1}{r}\sum_{j=1}^{r} T_j^2 - \frac{T^2}{k \cdot r}; \quad SS_e = \sum_{i=1}^{k}\sum_{j=1}^{r} X_{ij}^2 - \frac{1}{r}\sum_{i=1}^{k} T_i^2, \quad (2)$$

and

$$T = \sum_{i=1}^{k} T_i = \sum_{i=1}^{k}\sum_{j=1}^{r} X_{ij}. \quad (3)$$

When $F > F_{P \leqslant 0.05}(k-1, k(r-1))$, factor A is significant to the observations ($M_r{}^{cr}$).

Table 3. Orthogonal regression designs and the output power of the motor (obtained using a bi-section algorithm).

Sample No.	T	n_i	N	$M_r{}^{cr}$ (meV)
1	500 K	(20,20)/(25,25)	4	525
2	500 K	(20,20)/(25,25)	1	125
3	500 K	(9,9)/(14,14)	4	279.8
4	500 K	(9,9)/(14,14)	1	62.5
5	100 K	(20,20)/(25,25)	4	450
6	100 K	(20,20)/(25,25)	1	110
7	100 K	(9,9)/(14,14)	4	250
8	100 K	(9,9)/(14,14)	1	52.5

3. Numerical tests and discussion

3.1. Single factor analyses

As mentioned above, three major factors—i.e., temperature, the diameter of the rotor and the number of IRD atoms—are analyzed to find their significance to the output torque. Using a bi-section algorithm, we can obtain the critical value of the resistant torque moment of a nanomotor at the level of each individual factor. According to the results of the resistant torque, the relationship between the output torque (minus the resistant torque) and each factor is captured by a fitting approach. For example, to show the significance of temperature on the output power of the thermal nanomotor from CNTs (5,5)/(10,10), we firstly calculate the critical values of resistant torque at six different temperatures through a bi-section algorithm. Figure 2 illustrates the iteration histories of the resistance at the six levels, i.e., from 100 K to 600 K with increments of 100 K. For example, in the case of the rotor at 100 K, the rotational frequency of the rotor is $\sim$−368.44 GHz (clockwise) if there is no external resistance applied to it (figure 3). When we apply a resistant torque of $M_r = 30$ meV (i.e., 0.03 eV) to the rotor, the final SRF of the rotor is $\sim$−75.22 GHz (clockwise), which implies that its rotational direction is the same as that of the rotor without external

Table 4. Results of the analysis of variance (ANOVA) of the regression model by SAS software; DOF for degrees of freedom, SS for square summation, and MS for mean square. The F value can be obtained via equation (1).

Observation	Source	DOF	ANOVA SS	MS	F value	P value
M_r^{cr}	Model	6	0.223 063	0.037 177	184.04	0.0564
	Error	1	0.000 202	0.000 202		
	Sum	7	0.223 265		$R^2 = 0.999\,095$	

resistance ($M_r = 0$ meV). The value of ω is ~232.56 GHz when the resistant torque is of 40 meV. The rotational direction of the rotor is anticlockwise; this means that the resistance is too large to drive the rotor rotating in the opposite direction. Hence, the critical value of the resistant torque on the rotor at 100 K must be between 30 and 40 meV. After two iterations, the value of M_r^{cr} is found, i.e., $c = 0.5(a2 + b2) = 0.5(a2 + b1) = 32.5$ meV, at which the rotational frequency of the rotor is ~−0.37 GHz , i.e., ~0.1% of −368.44 GHz when $M_r = 0$ meV.

After obtaining the critical values of the resistant torque on the thermally driven nanomotor at different temperatures from 100 K–600 K, we establish the relationship between M_r^{cr} and T in the interval, as shown in figure 4(a). With the coefficient of determination of $R^2 = 0.957\,36$, M_r^{cr} is proportional to T with a slope of 0.01073 meV K^{-1}. Corresponding to the intercept of 28.057 33, the slope is too small, which indicates that the temperature in the interval of (100, 600) K has a slight influence on the output torque of the thermally driven nanomotor. Similarly, the relationship between M_r^{cr} and n_i (the chirality of the rotor in the nanomotor) or the number of IRD atoms on the stator can also be built. For instance, the relationship between M_r^{cr} (see supporting materials stacks.iop.org/NANO/28/215705/mmedia) and n_i shown in figure 4(b) indicates that the slope is of 11.61 meV. This demonstrates that the output torque of the motor is obviously enhanced when we choose a nanomotor from DWNTs with larger diameters. In figure 4(c), the relationship between M_r^{cr} and N is given. Clearly, the slope of 69.64 meV demonstrates that the output torque can be improved by placing more IRD atoms in the system. From the single factor analyses, a conclusion can be drawn that the output torque of a thermally driven nanomotor depends seriously on the diameters of the rotor and the number of IRD atoms, but only slightly on the variation of temperature in the interval (100, 600) K.

3.2. Multiple regression analysis

If we need a thermally driven nanomotor with adjustable output power, the interaction effects on the factors, e.g., the temperature, the diameter of the rotor and the IRD atoms on the output, have to be considered simultaneously. To estimate the interaction effect, orthogonal regression design/experiments for multi-factor analysis are employed. From the results of single factor analyses, and considering the computational costs, we know that the temperature has a weak influence, while n_i and N has a significant influence on the output torque of the motor. Hence, we conclude that the interaction effect must exist between n_i and N. Accordingly, the orthogonal design table is established by considering all three factors (T, n_i and N) and the interaction effects among any two of the three. Mathematically, the multiple polynomial regression model reads

$$y = \beta_1 x_1 + \beta_2 x_2 + \beta_3 x_3 + \beta_{12} x_1 x_2 + \beta_{23} x_2 x_3 + \beta_{13} x_1 x_3 + \varepsilon \tag{4}$$

where x_1, x_2 and x_3 are the coding values of the level of T, n_i and N, respectively (table 1). β_1, β_2 and β_3 are the main coefficient effects, and β_{12}, β_{13} and β_{23} are interaction coefficient effects; ε is the random error. The detailed design of the orthogonal regression experiments are given in table 2, and the critical values of the output power of the motor are listed in table 3 with respect to the eight samples. According to the values listed in table 1, the relationships between the coding values and the values of the factors can expressed as

$$x_1 = \frac{T - (T_2 + T_1)/2}{(T_2 - T_1)/2} = \frac{T - 300}{200},$$
$$x_2 = \frac{n_i - (n_{i2} + n_{i1})/2}{(n_{i2} - n_{i1})/2} = \frac{n_i - 14.5}{5.5},$$
$$x_3 = \frac{N - (N_2 + N_1)/2}{(N_2 - N_1)/2} = \frac{N - 2.5}{1.5}. \tag{5}$$

Table 5. The results of ANOVA of each factor or interaction of two factors.

Observation	Source	DOF	MS	F value	P value
M_r^{cr}	T	1	0.002 106	10.43	0.1912
	n_i	1	0.039 931	197.68	0.0452
	N	1	0.166 695	825.20	0.0222
	$T \times n_i$	1	0.000 315	1.56	0.4299
	$T \times N$	1	0.013 219	65.44	0.0783
	$n_i \times N$	1	0.000 796	3.94	0.2971

From table 4, we know that the difference between the coefficient of determination and 1.0 is no more than 0.1%. However, the P value is 0.0564—i.e., more than 0.05—which indicates that the significance of the regression equation (4) is weak, owing to the consideration of some insignificant factors. To overcome this problem, we calculate the F and P values of each factor in ANOVA as shown in table 5. It can be found that the P values with respect to factors T, $T \times n_i$, $T \times N$ and $n_i \times N$ are higher than 0.05. According to the rule of the stepwise regression approach [38], we firstly remove the factor $T \times n_i$, because the related P value is the maximum among the four cases. The major reason for this is that the

Table 6. Results of ANOVA of the modified regression model.

Observation	Source	DOF	ANOVA SS	MS	F value	P value
M_r^{cr}	Model	5	0.222 748	0.044 549	172.34	0.0058
	Error	2	0.000 517	0.000 258		
	Sum	7	0.223 265		$R^2 = 0.997\,684$	

Table 7. The results of the ANOVA of single factors in the modified regression model.

Observation	Source	DOF	MS	F value	P value
M_r^{cr}	T	1	0.002 106	8.15	0.1040
	n_i	1	0.039 931	154.47	0.0064
	N	1	0.166 695	644.84	0.0015
	$T \times N$	1	0.000 796	3.08	0.2214
	$n_i \times N$	1	0.013 219	51.14	0.0190

length of the stator is short and all the atoms on the stators are fixed during simulation, which results in the collision between the rotor and stator, and has no obvious improvement at higher temperatures. In this case, the modified regression model becomes

$$M_r^{cr} = \beta_1 x_1 + \beta_2 x_2 + \beta_3 x_3 + \beta_{23} x_2 x_3 + \beta_{13} x_1 x_3 + \varepsilon. \quad (6)$$

The ANOVA results are listed in table 6. Now the P value is far less than 0.05, and the F values are even higher than 100, with the coefficient of determination higher than 0.9997. Hence, the proposed regression model in equation (6) is reasonable, and the coefficients are given in the following equation:

$$M_r^{cr} = 0.016\,23 x_1 + 0.070\,65 x_2 + 0.144\,35 x_3 + 0.040\,65 x_2 x_3 + 0.009\,98 x_1 x_3 + 0.231\,85\ \text{eV}. \quad (7)$$

To show the significance of each factor in the modified regression model, the F and P values of ANOVA are listed in table 7. From table 7, the significance of the factors in the model are sorted, i.e., $F(N) > F(n_i) > F(n_i \times N) > F(\text{T}) > F(T \times N)$. This demonstrates that the number of IRD atoms N makes the highest contribution to the output power of the thermally driven nanomotor. The second major contribution to the output power should be the diameter of the rotor. However, the output power depends slightly on T or the interaction between T and N. Hence, the output power shows robustness with respect to temperature [39]. From the above analysis, the conclusion can be made that the output power of a motor can be improved significantly by adjusting the value of N or n_i, or both of them. This is helpful for the design of the thermally driven nanomotor from CNTs.

Substituting equation (5) into equation (6), we obtain the relationship between the output power and the factors as follows:

$$M_r^{cr} = -0.002 \times T + 0.5268 \times n_i + 14.805 \times N + 4.9273 \times n_i \times N + 0.0333 \times T \times N - 15.76\ \text{meV} \quad (8)$$

4. Conclusions

Multi-factor significance analysis of the output power of a thermally driven rotary nanomotor from CNTs is carried out by numerical experiments. In particular, the effects of temperature, the diameter of the rotor, and the number of IRD atoms (N) on a stator on the output power of the nano-system are investigated. Using stepwise regression analysis, the significance of each factor and the interaction effect between any two of the three are obtained. According to the ANOVA results, we discover that the value of N has the greatest influence on the output power (torque moment). The second and the third main factors that affect the output power are the diameter of the rotor and the interaction between N and the diameter. The temperature between 100 K and 500 K has a slight influence on the output power of the present nanomotor. The interaction between the temperature and N or the diameter is also relatively weak. The conclusion can be taken as guidance for the design of a rotary nanomotor whose output power can be controlled by adjusting the number of IRD atoms on the stator or the diameter of the CNTs.

Acknowledgements

J S is grateful for financial support from the Research Foundation for PhD in Northwest A&F University (Grant No 2452016176).

References

[1] Cumings J and Zettl A 2000 Low-friction nanoscale linear bearing realized from multiwall carbon nanotubes *Science* **289** 602–4
[2] Fennimore A, Yuzvinsky T, Han W-Q, Fuhrer M, Cumings J and Zettl A 2003 Rotational actuators based on carbon nanotubes *Nature* **424** 408–10
[3] Wu Z G, Wu Y J, He W P, Lin X K, Sun J M and He Q 2013 Self-propelled polymer-based multilayer nanorockets for transportation and drug release *Angew. Chem. Int. Ed.* **52** 7000–3
[4] Qiu W, Li Q, Lei Z K, Qin Q H, Deng W L and Kang Y L 2013 The use of a carbon nanotube sensor for measuring strain by micro-Raman spectroscopy *Carbon* **53** 161–8
[5] Wang Z, Jia H, Zheng X, Yang R, Wang Z, Ye G, Chen X, Shan J and Feng P X-L 2015 Black phosphorus nanoelectromechanical resonators vibrating at very high frequencies *Nanoscale* **7** 877–84
[6] Kroto H W, Heath J R, Obrien S C, Curl R F and Smalley R E 1985 C_{60}: Buckminsterfullerene *Nature* **318** 162–3
[7] Iijima S 1991 Helical microtubules of graphitic carbon *Nature* **354** 56–8

[8] Novoselov K S, Geim A K, Morozov S V, Jiang D, Zhang Y, Dubonos S V, Grigorieva I V and Firsov A A 2004 Electric field effect in atomically thin carbon films *Science* **306** 666–9
[9] Jiang J W and Park H S 2014 Negative Poisson's ratio in single-layer black phosphorus *Nat. Commun.* **5** 4727
[10] Cai K, Wan J, Wei N, Cai H and Qin Q H 2016 Thermal stability of a free nanotube from single-layer black phosphorus *Nanotechnology* **27** 235703
[11] 2016 (http://nobelprize.org/nobel_prizes/chemistry/laureates/2016/press.html)
[12] Bichoutskaia E, Heggie M I, Popov A M and Lozovik Y E 2006 Interwall interaction and elastic properties of carbon nanotubes *Phys. Rev.* B **73** 045435
[13] Zhang H, Cai K and Wang L 2008 Deformation of single-walled carbon nanotubes under large axial strains *Mater. Lett.* **62** 3940–3
[14] Zhang R, Ning Z, Zhang Y, Zheng Q, Chen Q, Xie H, Zhang Q, Qian W and Wei F 2013 Superlubricity in centimetres-long double-walled carbon nanotubes under ambient conditions *Nat. Nanotechnol.* **8** 912–6
[15] Cook E H, Buehler M J and Spakovszky Z S 2013 Mechanism of friction in rotating carbon nanotube bearings *J. Mech. Phys. Solids* **61** 652–73
[16] Zou J, Ji B, Feng X-Q and Gao H 2006 Self-assembly of single-walled carbon nanotubes into multiwalled carbon nanotubes in water: molecular dynamics simulations *Nano Lett.* **6** 430–4
[17] Bourlon B, Glattli D C, Miko C, Forró L and Bachtold A 2004 Carbon nanotube based bearing for rotational motions *Nano Lett.* **4** 709–12
[18] Barreiro A, Rurali R, Hernandez E R, Moser J, Pichler T, Forro L and Bachtold A 2008 Subnanometer motion of cargoes driven by thermal gradients along carbon nanotubes *Science* **320** 775–8
[19] Wang B, Vuković L and Král P 2008 Nanoscale rotary motors driven by electron tunneling *Phys. Rev. Lett.* **101** 186808
[20] Zambrano H A, Walther J H and Jaffe R L 2009 Thermally driven molecular linear motors: a molecular dynamics study *J. Chem. Phys.* **131** 241104
[21] Hamdi M, Subramanian A, Dong L, Ferreira A and Nelson B J 2013 Simulation of rotary motion generated by head-to-head carbon nanotube shuttles *IEEE/ASME Trans. Mechatronics* **18** 130–7
[22] Qiu W, Kang Y L, Lei Z K, Qin Q H and Li Q 2009 A new theoretical model of a carbon nanotube strain sensor *Chin. Phys. Lett.* **26** 080701
[23] Zheng Q and Jiang Q 2002 Multiwalled carbon nanotubes as gigahertz oscillators *Phys. Rev. Lett.* **88** 045503
[24] Legoas S, Coluci V, Braga S, Coura P, Dantas S and Galvao D 2003 Molecular-dynamics simulations of carbon nanotubes as gigahertz oscillators *Phys. Rev. Lett.* **90** 055504
[25] Guo W, Guo Y, Gao H, Zheng Q and Zhong W 2003 Energy dissipation in gigahertz oscillators from multiwalled carbon nanotubes *Phys. Rev. Lett.* **91** 125501
[26] Cai K, Yin H, Qin Q H and Li Y 2014 Self-excited oscillation of rotating double-walled carbon nanotubes *Nano Lett.* **14** 2558–62
[27] Leng J, Guo Z, Zhang H, Chang T, Guo X and Gao H 2016 Negative thermophoresis in concentric carbon nanotube nanodevices *Nano Lett.* **16** 6396–402
[28] Cai K, Li Y, Qin Q H and Yin H 2014 Gradientless temperature-driven rotating motor from a double-walled carbon nanotube *Nanotechnology* **25** 505701
[29] Cai K, Yu J, Yin H and Qin Q H 2015 Sudden stoppage of rotor in a thermally driven rotary motor made from double-walled carbon nanotubes *Nanotechnology* **26** 095702
[30] Cai K, Wan J, Qin Q H and Shi J 2016 Quantitative control of a rotary carbon nanotube motor under temperature stimulus *Nanotechnology* **27** 055706
[31] Cai K, Yu J, Wan J, Yin H, Shi J and Qin Q H 2016 Configuration jumps of rotor in a nanomotor from carbon nanostructures *Carbon* **101** 168–76
[32] Cai K, Yu J, Shi J and Qin Q H 2016 A method for measuring rotation of a thermal carbon nanomotor using centrifugal effect *Sci. Rep.* **6** 27338
[33] Cai K, Yu J, Liu L, Shi J and Qin Q H 2016 Rotation measurements of a thermally driven rotary nanomotor with a spring wing *Phys. Chem. Chem. Phys.* **18** 22478–86
[34] Zhu S and Li T 2014 Hydrogenation-assisted graphene origami and its application in programmable molecular mass uptake, storage, and release *ACS Nano* **8** 2864–72
[35] Yuan Y 2011 Multiple imputation using SAS software *J Stat. Softw.* **45** 1–25
[36] Plimpton S 1995 Fast parallel algorithms for short-range molecular dynamics *J. Comput. Phys.* **117** 1–19
[37] Stuart S J, Tutein A B and Harrison J A 2000 A reactive potential for hydrocarbons with intermolecular interactions *J. Chem. Phys.* **112** 6472–86
[38] Templ M, Kowarik A and Filzmoser P 2011 Iterative stepwise regression imputation using standard and robust methods *Comput. Stat. Data Anal.* **55** 2793–806
[39] Cai K, Yu Y J, Shi J and Qin Q H 2017 Robust rotation of rotor in a thermal driven nanomotor *Sci. Rep.* **7** 46159